Synergistic PAN/LiF Hybrid Layer Enabling Highly-Stable Lithium Metal Anodes via In-Situ Interface Engineering

Xianchao Zhao,[a] Weimin Chen,[a,*] Kang Huang,[a] Lanying Chen,[a] Hong Chen,[a] Yuyu Li,[c] Liang Wang,[b,*] Faquan Yu[a,*]

[a] Key Laboratory for Green Chemical Process of Ministry of Education, Hubei Key Laboratory for Novel Reactor and Green Chemistry Technology, School of Chemical Engineering and Pharmacy, Wuhan Institute of Technology, Wuhan 430205, China

E-mail: wmchen@wit.edu.cn; fyu@wit.edu.cn

[b] Chongqing Institute of Green and Intelligent Technology, Chinese Academy of Sciences, Chongqing 400714, China

E-mail: wangliang@cigit.ac.cn

[c] Laboratory of Flexible Optoelectronic Materials and Technology, Ministry of Education, Jianghan University, Wuhan 430056, China

Supporting information

1. Experimental Section

（1）Preparation of PAN/NH_4HF_2 precursor solutions

First, 0.04 g, 0.06 g and 0.08 g of NH_4HF_2, with three separate 0.06 g portions of polyacrylonitrile (PAN) powder were added to 2 ml of dimethyl sulfoxide (DMSO) solution and stirred until complete dissolution. The PAN/NH_4HF_2-*x* (where *x* represents the concentration of NH_4HF_2 in the solution) precursor solution was obtained. If not otherwise specified, the concentration of NH_4HF_2 was defaulted to be 0.03 g mL^{-1} in the following experiments.

（2）Preparation of PAN/LiF-Li electrode

The precursor solution was transferred into a glove box filled with argon (oxygen content ⩽0.01 ppm, water content⩽0.01 ppm). Before the in-situ reaction, the oxide layer on the Li foil was removed with a spatula, and about 300 μL of the precursor solution was added to the Li foil dropwise using a pipette. Then, the solution was spread out into a homogeneous film on the Li foil with a spatula, and the solution was left to react with Li in the presence of NH_4HF_2 at room temperature for 24 h. Finally, based on the reaction of NH_4HF_2 with Li that produces LiF, the Li metal anode with an organic/inorganic artificial interface layer was prepared.

2. Material characterization

The morphologies and structural characterizations of the as-obtained electrodes were investigated using field emission scanning electron microscopy (FESEM, Nova NanoSEM450) and X-ray diffractometer (XRD, Philips, with Cu-Ka is the radiation source, λ=0.15406 nm, the scanning rate of 5° min^{-1} and the scanning angle of 5°~90°). Energy dispersive X-ray spectrometer (EDX) and X-ray photoelectron spectroscopy (XPS,

AXISULTRADLD) were used to analyze the element distributions, content, and chemical states of the products. The FT-IR spectra were obtained on a JASCO FT/IR-4100 spectrometer.

3. Electrochemical measurements

The cycling performances were measured using the CR2032-type coin-cells assembled in an argon-filled glove box. The electrolyte was composed of 1.0 M $LiPF_6$ in EC/EMC (v/v=3:7). The separator is polypropylene membrane (Celgard, 2400 PP). Li||Li symmetric cells were configured with two identical bare Li foils, two PAN-Li or two PAN/LiF-Li as both the working and counter electrodes. Symmetric cells were applied to evaluate the polarization properties during Li stripping/plating under the constant current densities. Full cells were assembled to evaluate the feasibility of the PAN/LiF-Li anode. For the preparation of theLFP cathode, LFP powder, carbon black and polyvinylidene fluoride (PVDF) binder with a mass ratio of 7.5:1.5:1 was all dispersed in N-methyl-2-pyrrolidone (NMP) solvent. The slurry was casted onto Al foil and then dried at 60 °C for 24 h before assembling. The areal mass loading was 2 mg cm^{-2} for the cathode electrode. The galvanostatic charge-discharge processes were performed on Land CT2001A systems in a voltage range of 2.5−4.0 V (vs Li^+/Li). The electrochemical impedance spectroscopy (EIS) and cyclic voltammetry (CV) tests were conducted using the CHI 760E electrochemical workstation. Among them, the EIS measurement was probed over the frequency range of 100 KHz to 0.01 Hz, the CV curves were acquired using the LFP full cells at a scan rate of 0.1 mV s^{-1} between 2.5 and 4.0 V.

The Tafel curves of Li||Li symmetrical cells were measured at a scan rate of 1 mVs^{-1} from −0.15 to 0.15 V. The exchange current density was calculated based on Tafel equation.

$\eta = a + b\log(j)$ (Equation 1)

where j is the current density, η is the overpotential, a and b are constants.

The Li^+ diffusion coefficient of PAN/LiF-Li was measured by GITT. The PAN/LiF-Li||Cu cell was discharged/charged at a current density of 5 μA for 10 min, followed by an open circuit relaxation for 50 min, and such process was repeatedly conducted. The Li^+ diffusion coefficient was calculated based on the following equation:

$$D_{\mathrm{Li}} = \frac{4}{\pi\tau}\left(\frac{n_m V_m}{S}\right)^2\left(\frac{\Delta E_s}{\Delta E_t}\right)^2 \quad \text{(Equation 2)}$$

where τ (s) is the relaxation time, nm (mol), and Vm ($cm^3\ mol^{-1}$) are the molar mass and volume of PAN/LiF-Li, S is the electrode surface area, ΔE_s (V) is the voltage variation during current pulse, and ΔE_t (V) is the voltage change during the discharge/charge processes.

4. **Calculation method**

Atomic Simulation Environment (ASE) package[1] was employed for structure construction and calculation flow management. Vienna Ab-initio simulation package (VASP) was called for energies and forces calculation, which is based on density functional theory (DFT) and with frame of planewave-pseudopotential (PP)[2] and Projector-augmented wave (PAW)[3] implemented. The ultrasoft Perdew-Burke-Ernzerh (PBE) pseudopotential in general gradient approximation (GGA)[4] were chosen for electronic exchange and correlation interaction. The plane wave cutoff energy was set to 400 eV. Spin-polarized calculations were performed for those open-shell systems. The k-point grid by Monkhorst-Pack scheme[5] for SCF and lattice-dynamical matrices is 8×10×1 for PAN×2 slab, LiF(110) slab and PAN×2- LiF(110) slab. The convergence threshold of energy and ionic force were set to 1×10^{-4} eV and 1×10^{-3} eV/ Å in electrons and ions relaxation. For all slab models, spaces between slabs or molecular were specified to be 20 Å to avoid interaction [6-9].

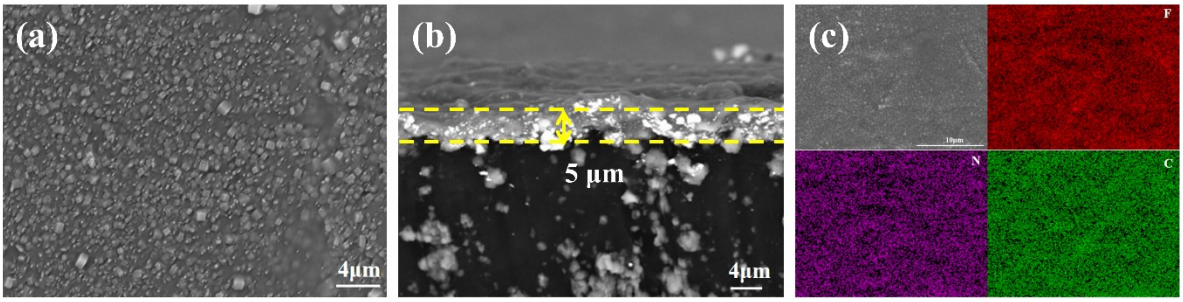

Fig. S1. SEM images of PAN/LiF-Li electrode: (a) surface, (b) cross-section; (c) surface morphology and corresponding C, N and F elemental distributions of PAN/LiF-Li electrode.

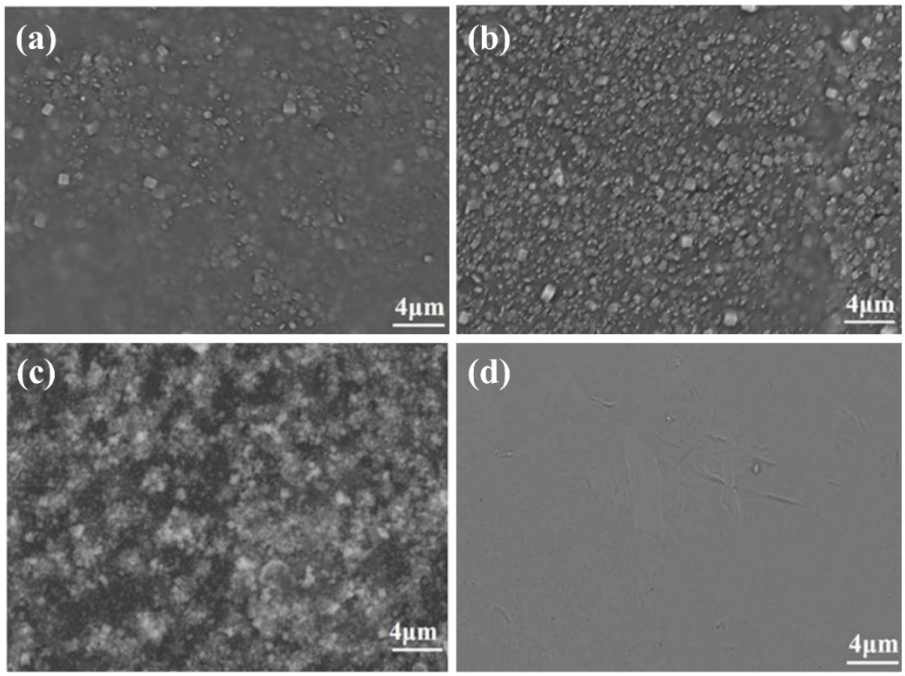

Fig. S2. The SEM images of different concentrations of precursor solutions after reaction with Li metal. (a) $\rho(NH_4HF_2)$ = 0.02 g mL^{-1}; (b) $\rho(NH_4HF_2)$ = 0.03 g mL^{-1}; (c) $\rho(NH_4HF_2)$ = 0.04 g mL^{-1}; (d) $\rho(NH_4HF_2)$ = 0 g mL^{-1}.

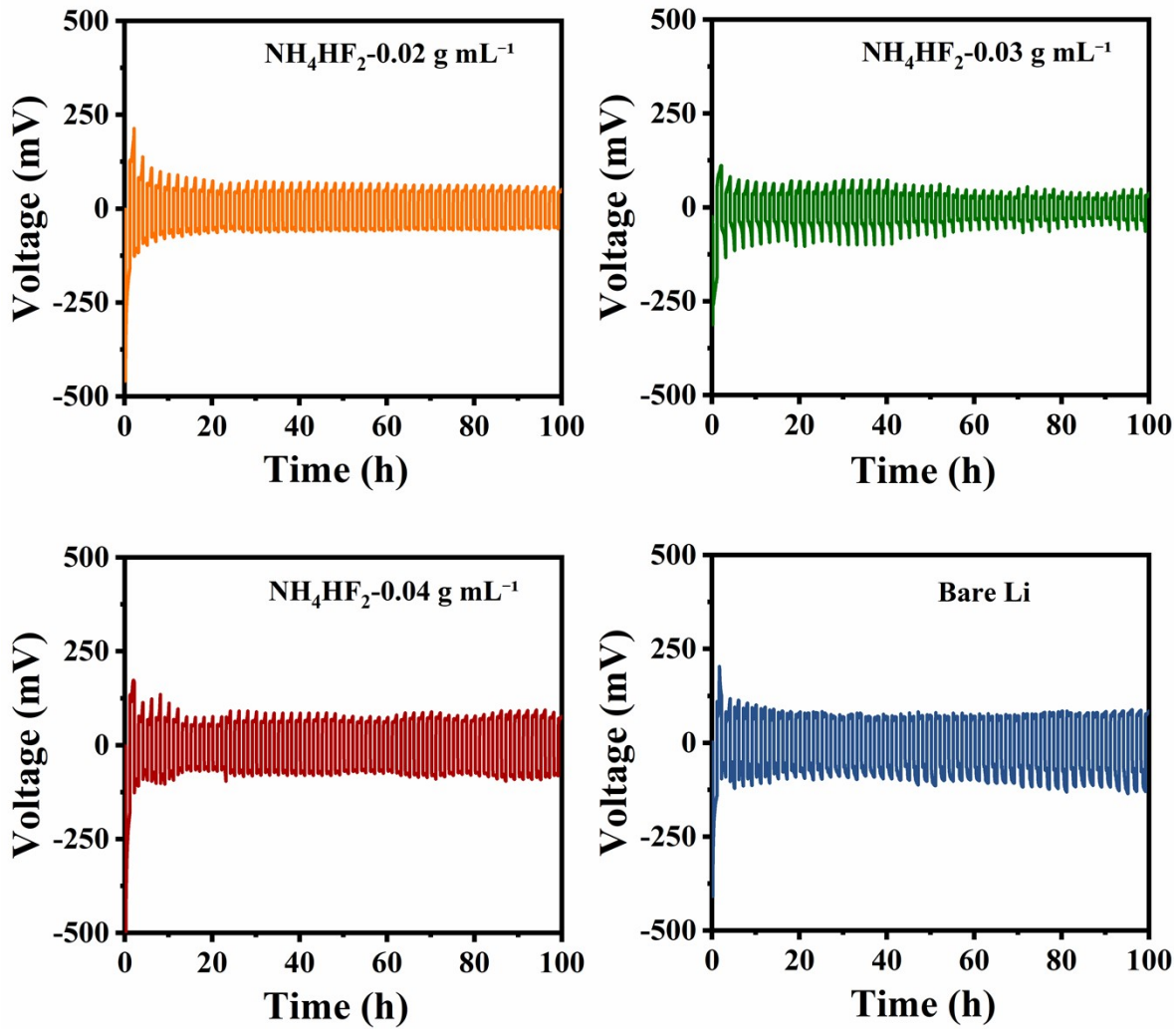

Fig. S3. Voltage-time profiles of the symmetric cells at 1 mA cm^{-2} and 1 mAh cm^{-2} with PAN/LiF-Li anodes prepared using different concentrations of precursor solutions: (a) $\rho(NH_4HF_2)$ = 0.02 g mL^{-1}; (b) $\rho(NH_4HF_2)$ = 0.03 g mL^{-1}; (c) $\rho(NH_4HF_2)$ = 0.04 g mL^{-1}; and (d) bare Li.

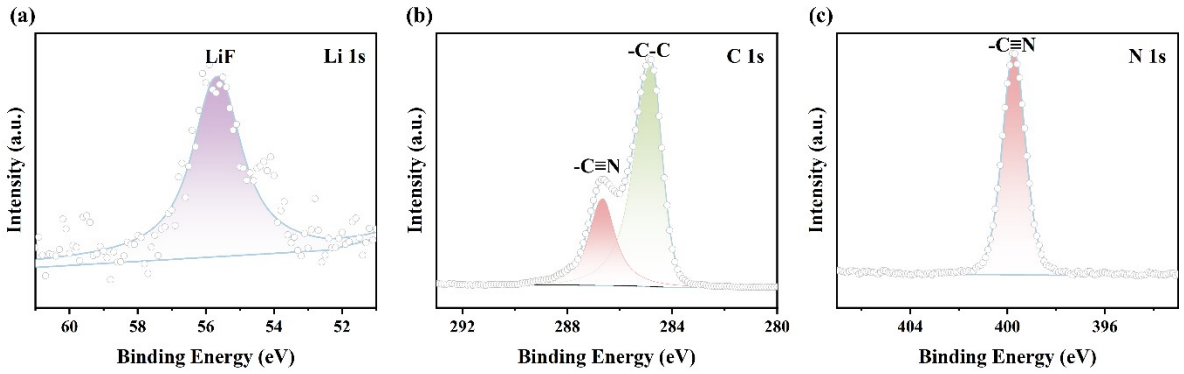

Fig. S4. High-resolution XPS spectra of PAN/LiF-Li for Li 1s, C 1s and N 1s.

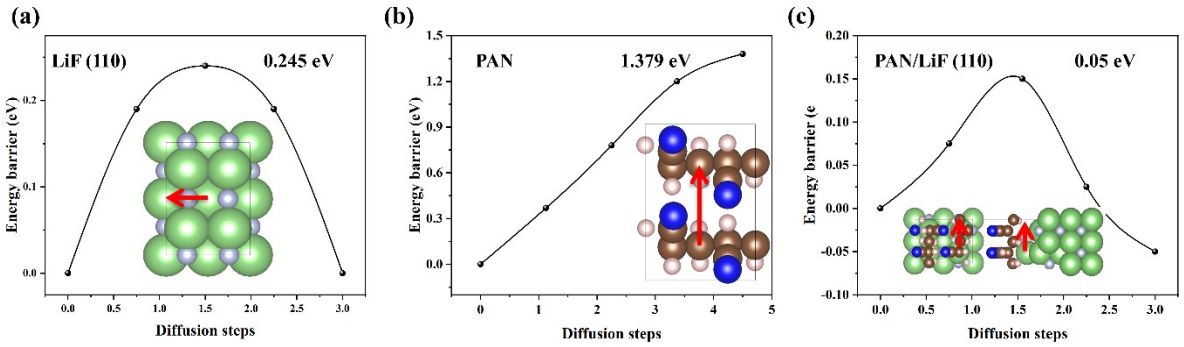

Fig. S5. Kinetic energy barriers of Li^+ diffusion on the (a) LiF (110), (b) PAN and (c) PAN/LiF (110) surfaces. The arrows represent the diffusion pathways on the surfaces.

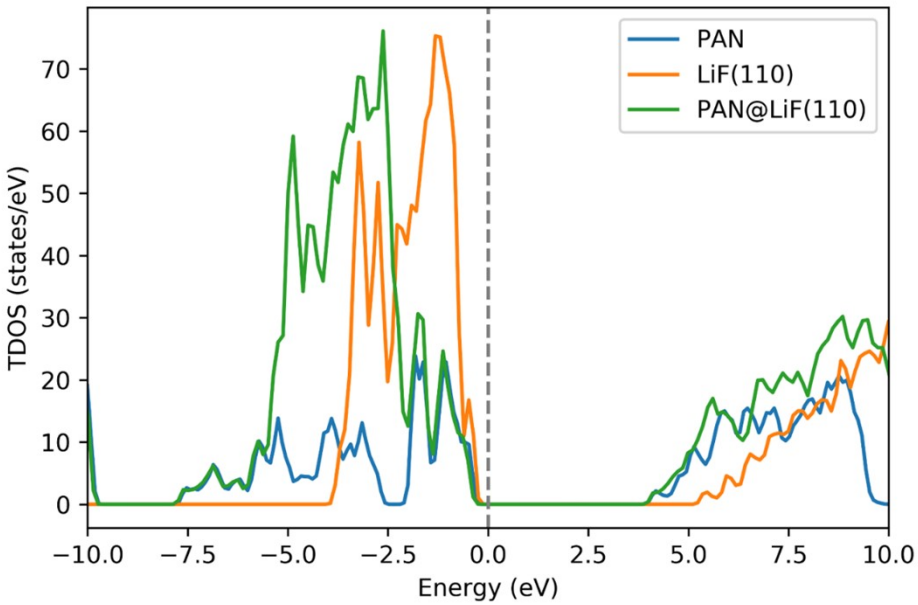

Fig. S6. Total density of states (TDOS) of PAN, LiF (110) and PAN/LiF (110) interfaces.

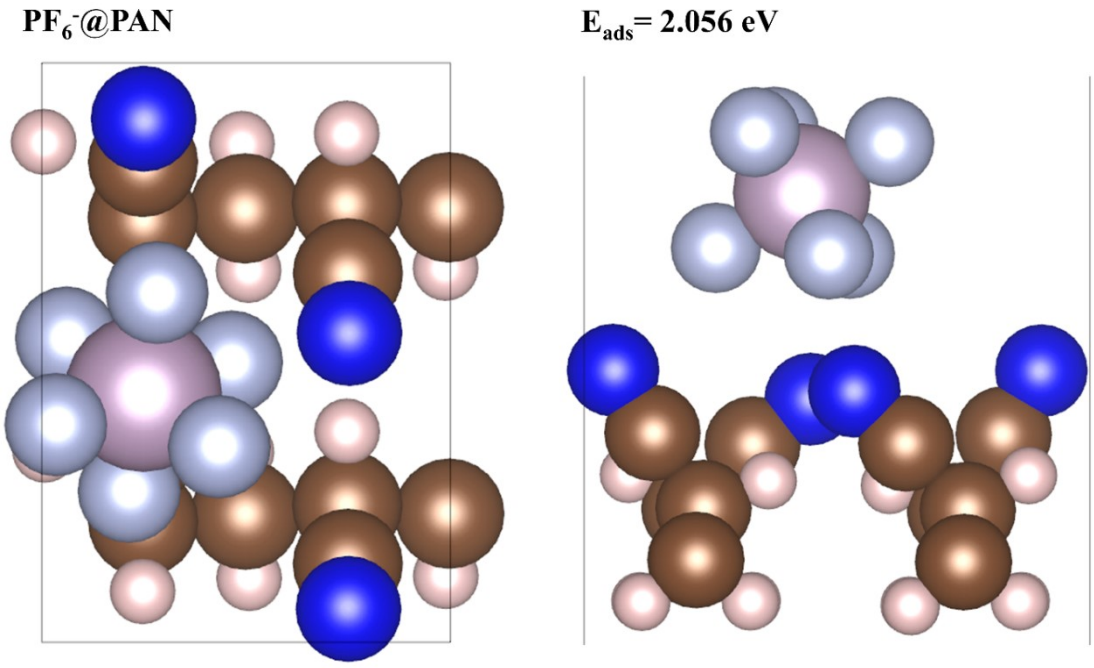

Fig. S7. Optimized adsorption configuration and adsorption energy of PF_6^- molecule on the PAN model.

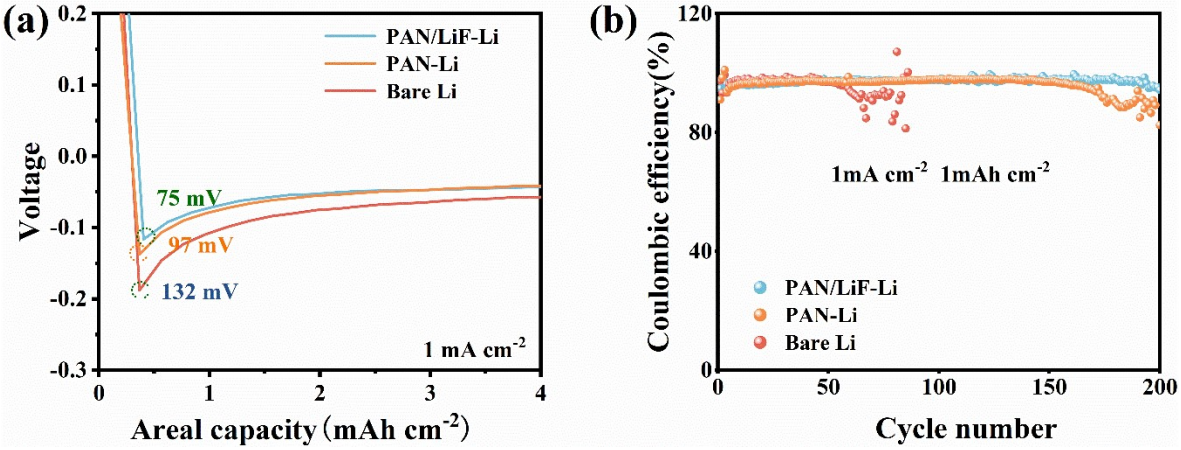

Fig. S8. (a) Initial Li plating voltage profiles of different nucleation overpotentials of bare Li foil, PAN-Li and PAN/LiF-Li electrodes at 1 mA cm^{-2}; (b) CE profiles of sample half-cells at 1 mA cm^{-2} with capacity of 1 mAh cm^{-2}.

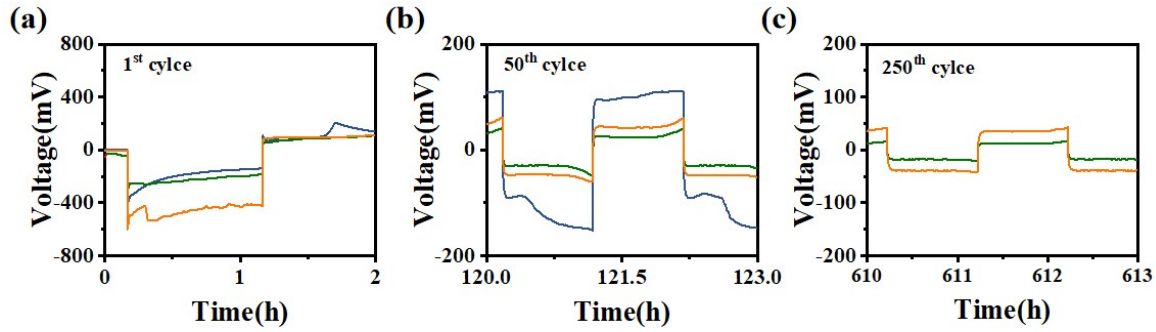

Fig. S9. Corresponding amplification voltage curves for three symmetric cells assembled with bare Li, PAN-Li, and PAN/LiF-Li anode electrodes, respectively, for different cycles at 3 mA cm^{-2} with capacity of 1 mAh cm^{-2}: (a) 1st cycle, (b) 50th cycle and (c) 250th cycle.

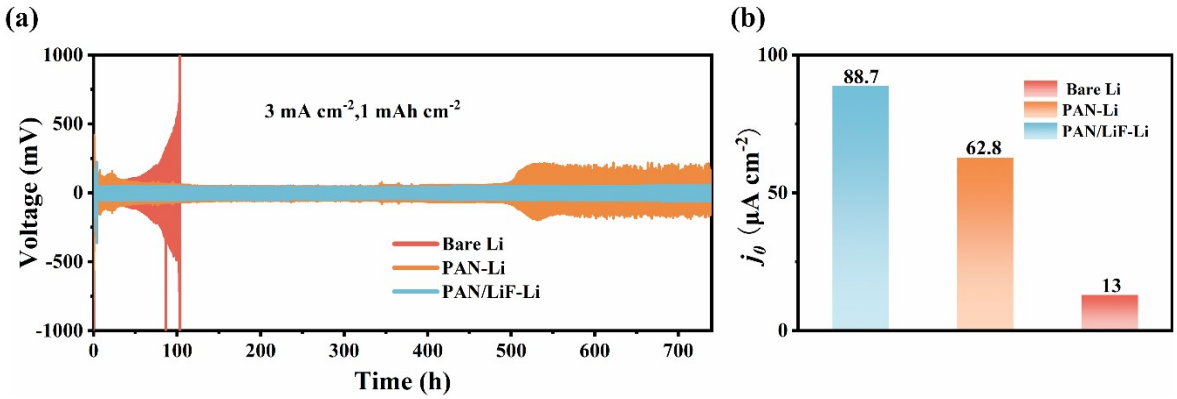

Fig. S10. (a) Voltage profiles of three symmetric cells assembled with bare Li, PAN-Li, and PAN/LiF-Li electrodes at 3 mA cm^{-2} with capacity of 1 mAh cm^{-2}; (b) calculated exchange current density of these symmetric cells.

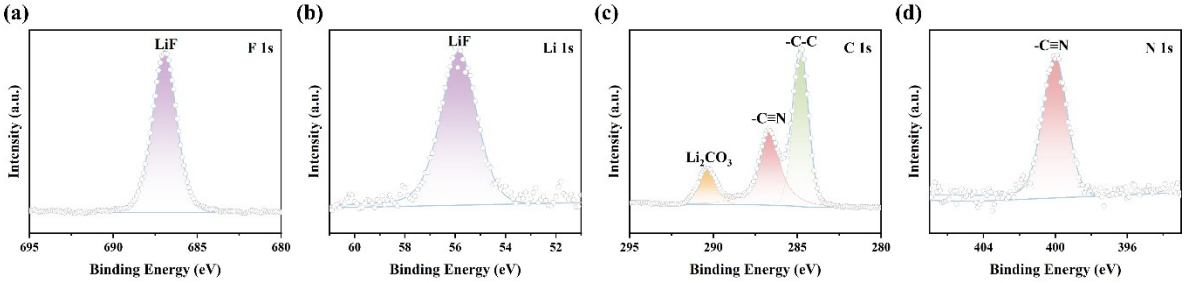

Fig. S11. XPS fine spectra of (a) F 1s, (b) Li 1s, (c) C 1s and (d) N 1s of the surface of PAN/LiF-Li electrode after cycling.

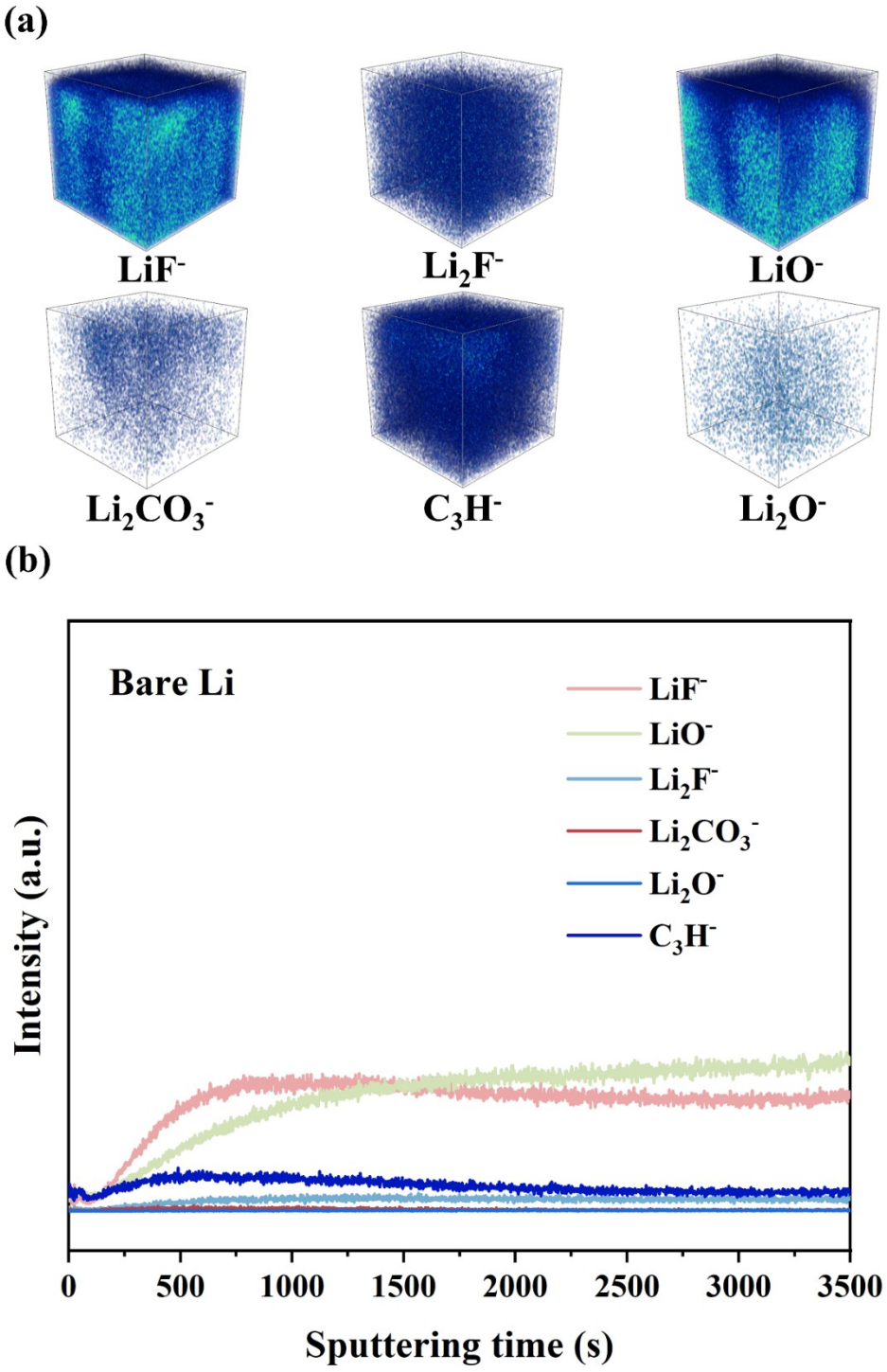

Fig. S12. After 100 plating/stripping cycles at 1 mA cm^{-2} and 0.5 mA h cm^{-2}, TOF-SIMS analysis of the bare Li surface: (a) 3D structural view of deep sputtering; (b) TOF-SIMS depth profile.

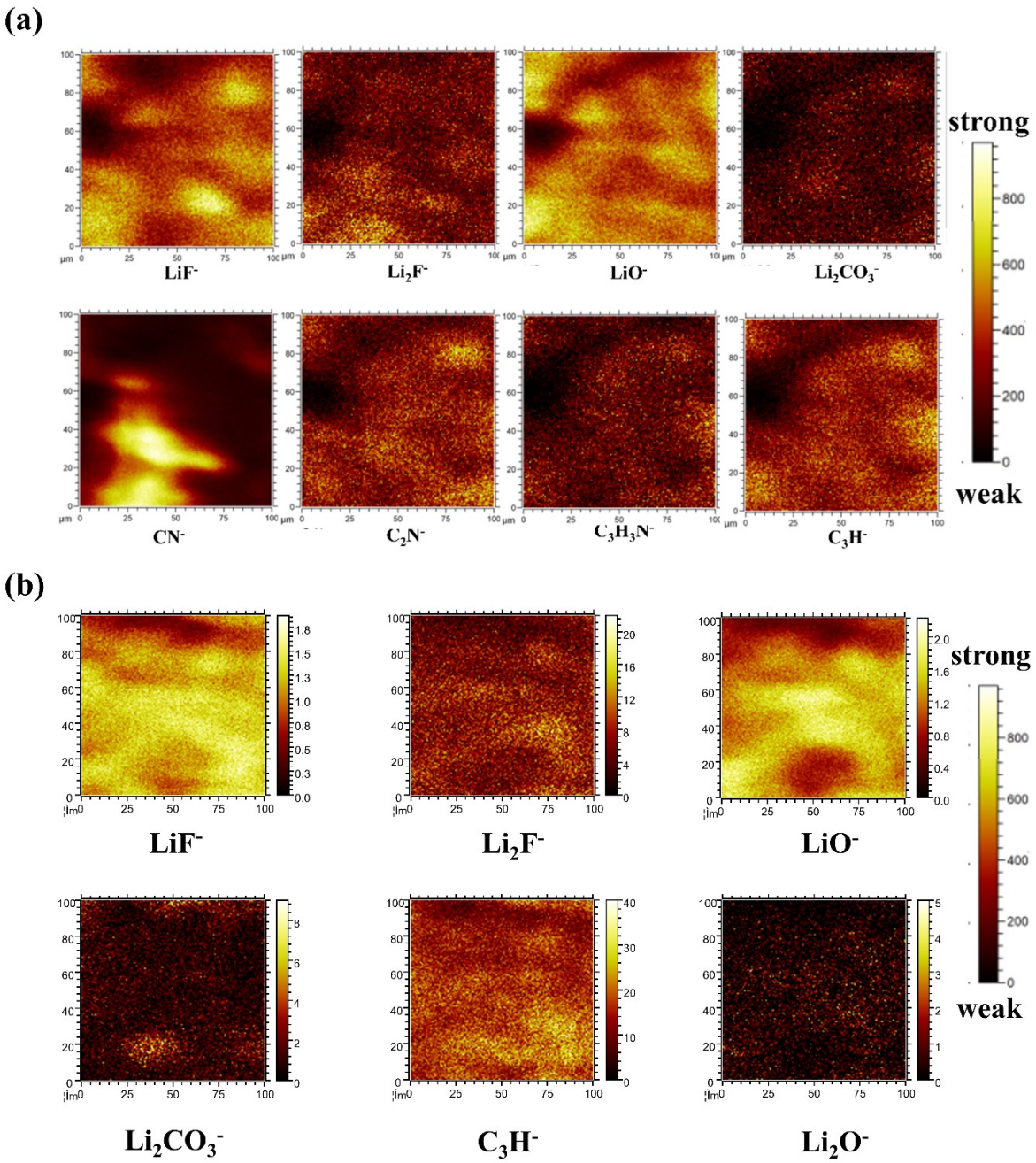

Fig. S13. Cross-profile images of TOF-SIMS depth sputtering in the surface of (a) PAN/LiF-Li and (b) bare Li electrode after 100 Li plating/stripping cycles at 1 mA cm^{-2} and 0.5 mA h cm^{-2}.

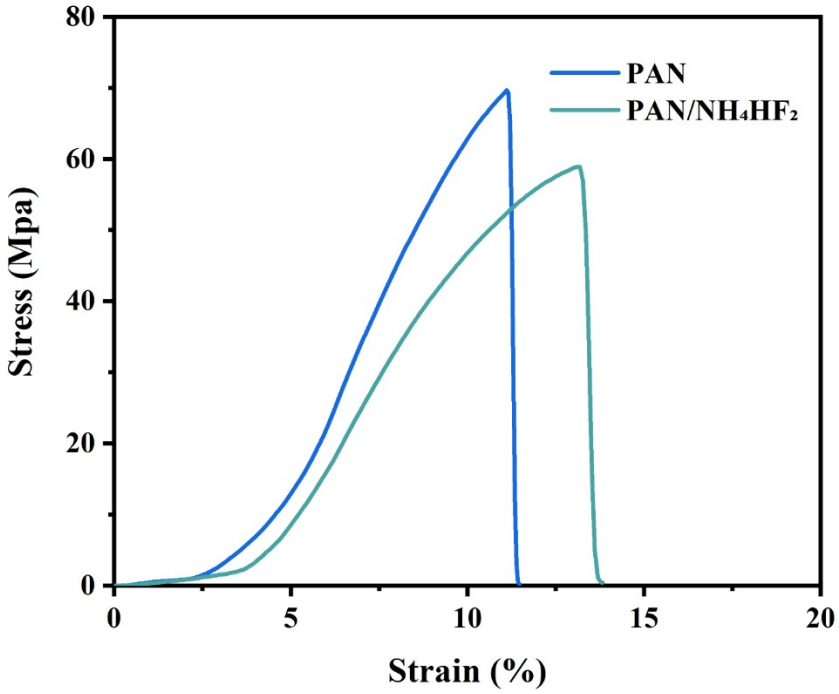

Fig. S14. Stress–strain curves of PAN and PAN/ NH_4HF_2.

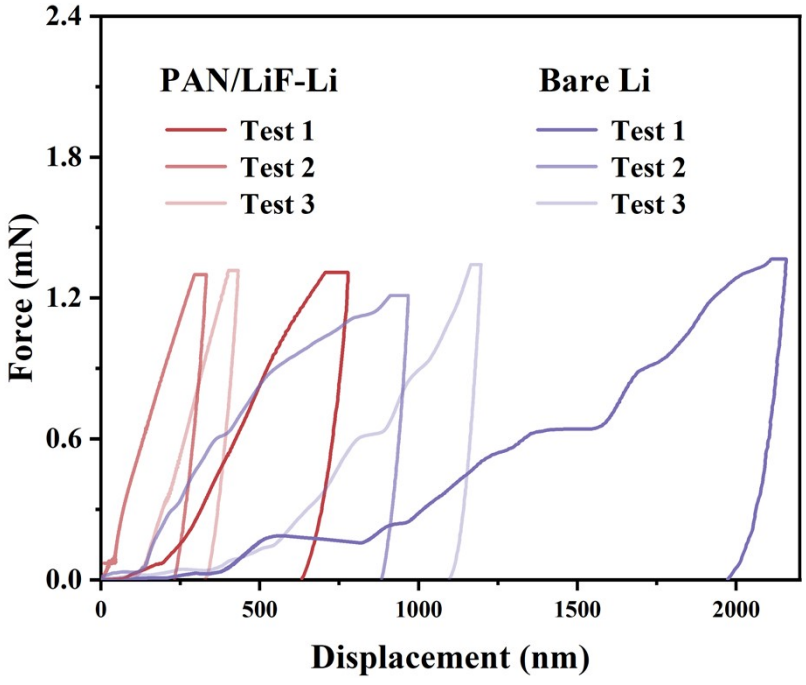

Fig. S15. Force-displacement curve from the Berkovich nanoindentation test for PAN/LiF-Li and bare Li anodes.

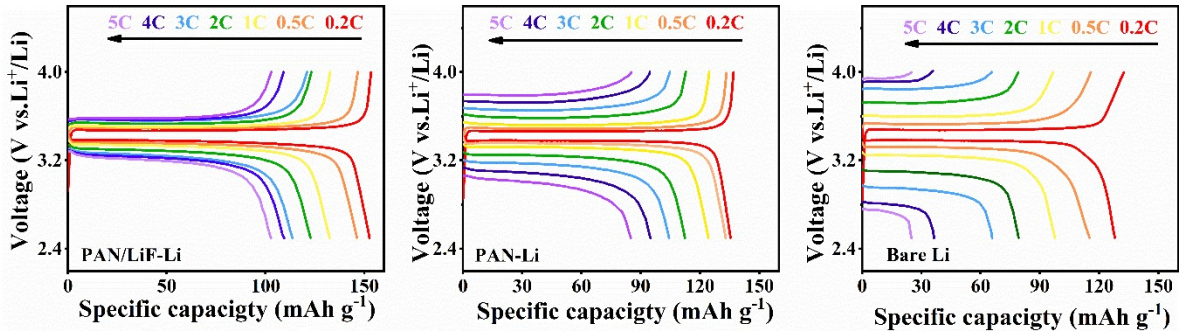

Fig. S16 The corresponding charge/discharge profiles at different current density of (a) PAN/LiF-Li||LFP; (b) PAN-Li||LFP; and (c) bare Li||LFP full cells.

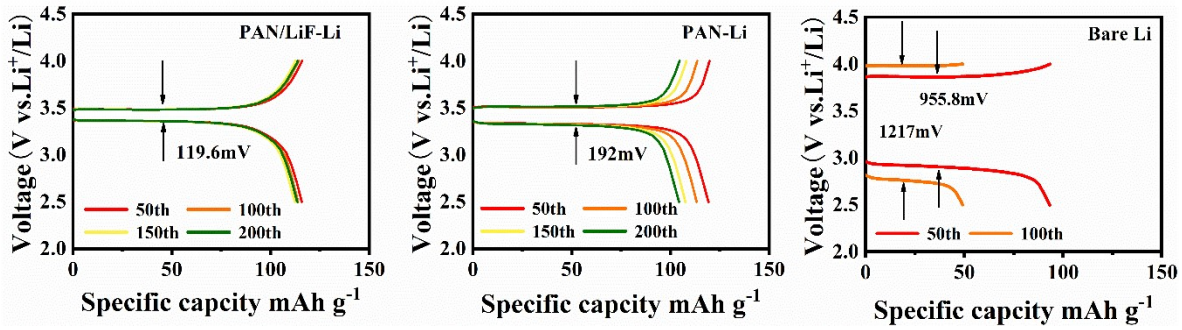

Fig. S17. The corresponding charge/discharge profiles of different cells at current density of 3 C: (a) PAN/LiF-Li||LFP; (b) PAN-Li||LFP; and (c) bare Li||LFP.

Table S1. Parameters of the PAN/LiF-Li ||NCM811 pouch cell.

Capacity	**176.3 mAh**
Cathode	**1.055 g**
Anode	**0.201 g**
Electrolyte	**0.88 g**
Separator	**0.13 g**
Mass	**2.266 g**

References

1. A. Hjorth Larsen, J. J. Mortensen, J. Blomqvist, I. E. Castelli, R. Christensen, M. Dulak, J. Friis, M. N. Groves, B. Hammer, C. Hargus, E. D. Hermes, P. C. Jennings, P. B. Jensen, J. Kermode, J. R. Kitchin, E. L. Kolsbjerg, J. Kubal, K. Kaasbjerg, S. Lysgaard, J. B. Maronsson, T. Maxson, T. Olsen, L. Pastewka, A. Peterson, C. Rostgaard, J. Schiotz, O. Schutt, M. Strange, K. S. Thygesen, T. Vegge, L. Vilhelmsen, M. Walter, Z. Zeng and K. W. Jacobsen, *J. Phys.-Condes. Matter.*, 2017, **29**.
2. S. Baroni, S. de Gironcoli, A. Dal Corso and P. Giannozzi, *Rev. Mod. Phys.*, 2001, **73**, 515-562.
3. P. E. Blochl, *Phys. Rev. B*, 1994, **50**, 17953-17979.
4. J. P. Perdew, K. Burke and M. Ernzerhof, *Phys. Rev. Lett.*, 1996, **77**, 3865-3868.
5. H. J. Monkhorst and J. D. Pack, *Phys. Rev. B*, 1976, **13**, 5188-5192.
6. L. F. Huang, P. L. Gong and Z. Zeng, *Phys. Rev. B*, 2014, **90**, 045409.
7. R. Beiranvand and S. Valedbagi, *Diam. Relat. Mater.*, 2015, **58**, 190-195.
8. L. H. Li, E. J. Santos, T. Xing, E. Cappelluti, R. Roldan, Y. Chen, K. Watanabe and T. Taniguchi, *Nano Lett.*, 2015, **15**, 218-223.
9. S. Thomas, K. M. Ajith and M. C. Valsakumar, *J. Phys. Condens. Matter.*, 2016, **28**, 295302.